STRUCTURAL CHANGES DURING THERMAL FATIGUE OF TWO NICKEL-BASED ALLOYS

P. C. Becker and J. Nutting

ABSTRACT

Thin-foil transmission electron microscopy was used to follow the changes in microstructure and dislocation morphology with increasing thermal cycling. Considerable carbide precipitation on dislocations occurred in both alloys during thermal cycling. Precipitate-free regions adjacent to grain boundaries in Nimonic 90 were also produced. Nimonic 90 exhibited high resistance to recovery at maximum cycle temperatures up to 900°C, while considerable recovery occurred in Nimonic 75. It is thought that the microstructural changes produced during thermal cycling as well as the ability of the alloy to recover, greatly affect the thermal endurance of these heat-resisting alloys.

P. C. Becker is a research metallurgist with the Republic Steel Corporation, Independence, Ohio.

J. Nutting is the Professor of Metallurgy, University of Leeds, Leeds, England.

INTRODUCTION

Among the multiplicity of components operating in conditions likely to cause thermal fatigue failure, the blading of aircraft gas turbines is of the greatest topical interest. The temperature of a turbine blade, especially the relatively thin edges, can change rapidly during use, because of the changing conditions associated with jet aircraft flight.

Nickel-based alloys are used for gas turbine blade material because of their combined high temperature strength and oxidation resistance. However, these materials are sometimes susceptible to thermal fatigue damage.

Because most thermal fatigue failures in service are caused by the repetition of thermal strains which result from temperature differences between various parts of a component when it is rapidly heated or cooled, Glenny et al.[1] designed an experiment that simulated the thermal stresses occurring in gas-turbine blades. Their experiment was used by Glenny and Taylor[2] to identify the significant factors governing the thermal fatigue behavior of a number of commercial nickel-chromium-based alloys. The tests were made by suddenly immersing tapered discs of the alloys alternately in hot and cold fluidized beds, each test being continued until a radial crack could be detected on the rim of the disc. (The tapered discs used in this test will henceforth be referred to as the National Gas Turbine Establishment (NGTE) specimens.) By thermally cycling all of the Nimonic series of alloys (up to Nimonic 105), the authors found that the maximum temperature of the cycle was a more influential factor than temperature range. Increase in the upper temperature generally reduced endurance values because of the diminshing strength of the material. However, above a critical maximum temperature, the effect of temperature on endurance diminished, probably owing to the increased ductility at these temperatures, which appeared to more than counterbalance the loss of strength. A metallographic study of these discs showed that thermal fatigue cracks originated at the surface and were intercrystalline in origin and mode of propagation, thus exhibiting the characteristics of creep rather than fatigue failure. Surface oxidation, which is intergranular in nature for nickel-based alloys, had a significant effect on thermal fatigue. The use of an argon atmosphere gave an appreciably longer endurance than an air atmosphere.

From the curves of thermal fatigue endurance versus maximum temperature of the cycle, the authors found that up to a temperature of 950°C the high strength alloys, Nimonic 100 and Nimonic 105, were superior to Nimonic 75. The endurances of Nimonics 100 and 105 diminished rapidly above 950°C to the level of the other precipitation hardenable alloys tested. Although Nimonic 75 (not a precipitation-hardenable alloy) showed a lower thermal endurance than the other materials, the differences were small above 1000°C. The variation, in order of merit, of these alloys appeared to be associated with their combined strength and ductility at the various testing temperatures.

Glenny[3], in his review of thermal fatigue, described the results of investigations which sought to determine the effects of maximum temperature, temperature range, and mean temperature on the thermal fatigue life of a number of high temperature materials. For most alloys, increasing the maximum temperature decreased the thermal endurance up to a critical maximum temperature. Above this temperature, the endurnace either no longer decreased, i.e., remained constant, or increased slightly. Glenny and Taylor viewed this as a consequence of increased ductility, while Baron and Bloomfield[4] reasoned that it was due to recrystallization. It would be expected that by increasing the temperature range, and therefore the thermal strain range, the thermal fatigue life would decrease. However, it was demonstrated by Glenny and Taylor and Clauss and Freeman[5] that the thermal endurance was more sensitive to maximum temperature than to temperature range or mean temperature.

Baron and Bloomfield[4] investigated the thermal fatigue behavior of some steels, high-temperature superalloys and cast irons. Their tests involved the repeated heating of the narrow edge of a continuously water-cooled, truncated, wedge-shaped specimen. They found that, in general, the alloys with the greatest hot strength were most resistant to cracking, provided the strains were not too large. However, when the strains were increased, it appeared that ductility was more important than strength. An annealing effect at peak temperature may be helpful, as indicated by the improvement of Nimonic 90 above a peak temperature of 900°C. A microscopic examination of the fracture of the Nimonic alloys showed transgranular cracking at lower temperatures, with a trend towards intergranular fracture with increasing temperature. Fracture at a maximum cycle temperature of 900°C was characterized by crack development both along grain boundaries and along slip lines. This transition in fracture mode with temperature is usually associated with creep.

Forrest and Armstrong[6,7] and Franklin et al.[8] concluded that the thermal fatigue resistance of a material was dependent upon the combination of strength and ductility throughout the whole temperature range of application. They showed that if a material could be rendered more ductile without loss of strength it would have increased thermal endurance. Franklin et al.[8] have derived an emperical equation relating thermal endurance to maximum cycle temperature and elevated-temperature yield strength and ductility. This equation agreed well with the observed results.

Some metallographic studies have been made on thermally fatigued Nimonics[1,2,8] and these have indicated that above a maximum cycle temperature of 800°C intergranular fractures predominated, while below this temperature transgranular fracture was usual. However, little research has been attempted to determine the fundamental causes of thermal fatigue in f.c.c. alloys.

A study has been made, therefore, using thin-foil transmission electron metallographic techniques of some of the basic metallurgical factors affecting thermal fatigue. It was hoped that by following the changes in density and distribution of dislocations, and by observing the changes in distribution of important microconstituents with increasing thermal damage, that it would be possible to gain some knowledge of the mechanism of thermal fatigue.

Two commercial nickel-based alloys, Nimonic 75 and Nimonic 90*, whose compositions are shown in Table I, were chosen for this investigation. Nimonic 75 is a solid solution strengthened material, while Nimonic 90 is a precipitation hardenable alloy. These alloys were chosen so that the effect of various hardening mechanisms could be related to thermal fatigue characteristics.

The investigation was divided into two segments: (1) The examination of unconstrained specimens and (2) the examination of constrained specimens which were tested to fracture.

EXPERIMENTAL TECHNIQUE

Unconstrained Specimens

To separate the metallurgical factors from the design factors responsible for thermal fatigue it was thought desirable to eliminate all extraneous constraints and environmental factors that may be responsible for damage. For this reason, thin circular specimens of uniform thickness were used which were thermally fatigued in an inert argon atmosphere. These specimens were 0.75 in. dia. x 0.020 in. thick and were cut from sheets of the two alloys. They were then given the appropriate heat treatments (see Table I). The specimens were loosely supported in a fused-silica holder and thermally cycled by heating rapidly to 900°C and then gas quenched to room temperature with cooled argon. A typical thermal cycle is shown in Figure 1. The maximum heating rate was 55°C/sec and the maximum cooling rate was 120°C/sec. Both alloys were thermally fatigued up to 1500 cycles.

Thin foils were made from thermally fatigued specimens by ultrasonically drilling 2.3 mm dia. discs and then electropolishing these discs in a PTFE holder[9]. After initial thinning in dilute HCl, final polishing and thinning were carried out in a solution of 5% perchloric acid - 95% acetic acid at 40-42 volts. The foils were examined in a Siemans Elmiskop Ia operated at 100 kv.

Constrained Specimens

Tapered disc specimens (NGTE specimens) of the two alloys were thermally fatigued to fracture in a fluidized bed apparatus at two different maximum cycle temperatures. The specimens and apparatus were

*Nimonic is a trade name of Henry Wiggin and Co., Ltd.

similar to those used by Glenny and Taylor[2] and all of these tests were performed at the International Nickel Co., Ltd., Birmingham, England. The major difference between the tapered disc specimens and the unconstrained specimens was that the former were subjected to both methcnical constraint and large thermal gradients, while the latter were not. Because these tapered disc specimens bear a great similarity to actual turbine blades, it was thought that valuable information could be obtained from their examination. The thermal cycle at the tapered edges of the specimen was similar to that shown in Figure 1.

Small discs suitable for electropolishing in the PTFE holder were spark-machined from material as close to the tapered edge as possible, since this was where severest thermal fatigue damage was observed. These discs were then electropolished and examined in the electron microscope. Where possible the fractured areas of these specimens were also examined optically.

RESULTS

Unconstrained Specimens

Much of this part of the investigation was reported in an earlier paper[10]. However, additional results were obtained after this publication. For completeness, these results are repeated along with the new findings.

Nimonic 75

The microstructure of a specimen of Nimonic 75 after heat treatment, but before thermal fatigue, consisted of a f.c.c. solid-solution matrix phase in the form of equiaxed grains and annealing twins, and a number of large particles of h.c.p. M_7C_3 at grain boundaries and within the grains. Dislocations were not observed in any specimens which were not subjected to thermal fatigue. This indicates that the initial dislocation density was low and that the ultrasonic drilling operation used for making 2.3 mm diameter discs did not introduce significant plastic deformation into the sample.

After a few thermal cycles, the dislocation density had already increased and pile-ups were present at twin and grain boundaries. A few sub-boundary networks were also present, indicating that some recovery had taken place. The origin of these dislocations may have been the twin and grain boundaries, but there was evidence that prismatic punching of dislocations from around the dispersed carbides was taking place (Figure 2), and since the density of dislocations around these carbides increased as the number of thermal cycles was raised (Figure 3) it is reasoned that the regions around these carbides are an important source of plastic deformation. The prismatic punching of dislocations occurs during rapid temperature changes since the coefficient of thermal expansion of the carbide is much lower than that of the matrix. Stresses are set up in the matrix areas adjacent to the carbides, and in

order to relieve these stresses, dislocations are produced as shown by Jones and Mitchell[29]. The large carbide particles can also act as barriers to dislocation movement. Dislocations would then accumulate at the carbide interfaces, concentrating much of the plastic deformation at the carbides. The dislocation density became greater with further cycling and it was possible for recovery to occur during the high-temperature segment of the cycle. Recovery networks were clearly visable after 100 cycles (Figure 4). These networks became more pronounced as the number of cycles was increased still further, and ultimately well-defined subgrains were formed after 1500 cycles (Figure 5). Usually the subgrains linked the intragranular carbides.

Vickers hardness measurements were taken after different numbers of thermal cycles. These indicated a very slight, but consistent, increase in hardness from $\sim$ 225 to 240 VHN.

Nimonic 90

Nimonic 90 is an age-hardenable alloy containing a fine dispersion of $Ni_3(Al,Ti)$ which has an ordered f.c.c. structure (γ'). This phase is coherent with the matrix, their lattice parameters being almost identical. Also present are large particles of a f.c.c. metallic carbide phase based on $Cr_{23}C_6$ and referred to as $M_{23}C_6$. Nimonic 90 is solution-treated at 1080°C for 8 hours in order to dissolve all existing γ', but this temperature is not high enough to fully dissolve the $M_{23}C_6$. It is then air cooled and aged for 16 hours at 700°C in order to produce a very fine dispersion of γ' particles having a diameter of 40-60 Å.

The carbide phase appears in two locations in the microstructure: at grain boundaries, as spheroids due to nucleation and growth, and as cells owing to discontinuous precipitation; and within the grains, as large spheroids (see Figure 6). Note, that no γ' depletion has occurred adjacent to the grain boundaries in both cases shown in Figure 6.

On thermal cycling, the γ' particles increased in size and had grown to $\sim$ 300 Å in dia. after 10 cycles. Dislocation generation occurred, as in the Nimonic 75, giving rise to high dislocation densities near the grain boundaries and the carbides (Figure 7). Plastic deformation of this alloy produced superlattice dislocations due to the shearing of the ordered γ' particles and these are clearly visable at A in Figure 7.

Further growth of the γ' particles occurred, after 20 cycles, producing particles $\sim$ 350 Å in diameter. Both superlattice dislocations and dislocation loops are present, indicating that two deformation mechanisms are acting at the same time[11,12]. Merrick[13] has indicated that there is a critical diameter of coherent precipitate particle above which the dislocations do not shear the γ' particles, but find it easier to by-pass the particles by bowing around them. This critical diameter was calculated to be approximately 280 Å, which compares favorably with the γ' diameter produced after 20 cycles since only some of the particles had loops around them.

Further growth of the γ' particles occurs with increasing numbers of cycles. The consequent increase in the interparticle spacing now allows the modes of dislocation movement to change. Thus, after 250 cycles no double dislocations are observed, while loops are very infrequent. The dislocations can move readily through the grains and form loose tangles outlining subgrains, as shown in Figure 8. The γ' particle diameter is now $\sim$ 520 Å. Increasing the number of cycles to 1500 led to still further growth of the γ' particles to a dia. of $\sim$ 800 Å. The dislocation density rose further and subgrains were formed, but these were never as clearly defined as in the Nimonic 75.

During the examination of thermally fatigues specimens, it was observed that the γ' particle diameter appeared to increase very rapidly with increasing numbers of thermal cycles. It was necessary, therefore, to ascertain whether this rapid growth was caused by the thermal cycling process or whether it was just a consequence of the high temperatures employed during cycling. Since the specimen remains at 900°C for 45 seconds of the total heating time of 2 minutes (Figure 1), it was assumed that one thermal cycle was approximately equivalent to a one minute soak at 900°C. A commercially heat treated specimen of Nimonic 90 was soaked for various periods of time at 900°C, so that the γ' particle diameter of the soaked specimen could be compared with the γ' diameter produced by thermal fatigue. The results are shown in Figure 9. It appears that thermal cycling has a profound effect on the early stages of coarsening of the γ' particles. This effect causes Nimonic 90 to age much more rapidly during thermal fatigue than during high temperature annealing for an equivalent period of time.

The γ' particle diameters for both types of specimens were determined mostly from bright field electron microscopy, although some dark field microscopy was also used. Because of the elastic strain fields associated with the coherent γ' particles, accurate particle diameter measurements were difficult to obtain. However, it was thought that if there was a substantial effect on particle growth caused by thermal fatigue then this method of measurement might suffice. By a comparison of micrographs from both specimens, it was found that although the exact values for γ' particle diameters may be in error, the effect of thermal cycling on particle growth can still be established, since the errors would be the same for both treatments.

The initial rapid growth rate can be explained as follows: When the specimen is soaked at 900°C, the γ' particles grow by the Ostwald ripening mechanism[14]. The small particles go back into solution and the large particles increase in size. This form of growth will also occur during the high temperature segment of the thermal cycle, but a further change can also occur. The equilibrium volume fraction of the precipitated γ' becomes greater as the temperature is reduced. Under these conditions the larger particles are likely to grow still more readily than the smaller ones, since the equilibrium solute concentration around the larger particles is always lower than around the smaller precipitates. On reheating, it is likely that the smaller

particles will be taken into solution faster than the larger ones. There is, therefore, a thermal ratcheting effect which favors the growth of the larger particles. However, this ratcheting effect appears to diminish as the mean particle size increases. The curves for the thermally cycled and constant temperature soaked specimens appear to coincide when the particle size becomes greater than 500 Å in diameter.

Ardell and Nicholson[15] have shown that γ' coarsening in a binary Ni-Al alloy is diffusion-controlled (Ostwald ripening), and obeys an r^3 vs t relationship. It would be of interest to determine whether the test specimens in this research follow such a relationship.

Wagner[16] has derived an expression for the coarsening of solid particles in a fluid phase, which states that the mean radius, $\bar{r}$, of a particle increases with time, t, according to the equation

$$\bar{r}^3 - \bar{r}_o^3 = \frac{8 \gamma D c_o V_m^2 t}{9RT} = kt$$

where

$\bar{r}_o$ = the mean value of r at the onset of coarsening.

D = the coefficient of diffusion of solute in the matrix.

γ = the specific interfacial free energy between the external phase and the particle of molar volume V_m.

R = universal gas constant.

T = temperature (^oK).

c_o = the equilibrium molar solubility of a particle of infinite radius in a given fluid phase.

This expression is valid only if the growth process is diffusion-controlled and only after a time when the matrix has been depleted of solute down to the concentration c_o. The equation predicts a linear relationship between $\bar{r}^3$ and t, with slope k and intercept $\bar{r}_o^3$.

The values of $\bar{r}^3$ and t were plotted for both the 900°C soaked and the thermally cycled specimens, and are shown in Figure 10. Since the value of $\bar{r}_o^3$ is so small, it was neglected. The graph shows a linear relationship between $\bar{r}^3$ and t for the soaked specimen, indicating that a diffusion-controlled mechanism may be operative for the γ' coarsening. This is to be expected in the light of the work of Mitchell[17], who studied the γ' coarsening at aging temperatures from 600°C to 1100°C of several Nimonic alloys, including Nimonic 90. He found that a diffusion-controlled mechanism was responsible for the coarsening of the γ' particles in all of the alloys. The fact that the values of γ' diameter measured in the present study also follow a straight line relationship indicates that they may not be too much in error, especially for large values. In order to check whether the straight line in

Figure 10 is a reasonably accurate measure of the growth characteristics of the γ', the slope, k, of the line should be determined and, from this value, D can be calculated. If this value approximates the value of D which has been determined experimentally, then the straight line is a valid expression of the growth characteristics of the γ'. A value for k of $1.63 \times 10^{-21} cm^3/sec$ was determined from the slope of the line. Ardell and Nicholson[15] have found that the value for γ for particles of Ni_3Al in a nickel-rich matrix was equal to about 30 ergs/cm^2. c_o can be calculated from the expression

$$c_o = \rho_X W_o / M_s$$

where:

ρ_X = density of matrix solid solution.

W_o = equilibrium weight fraction of solute in the matrix. This can be determined from the relevant portion of the phase diagram which represents the alloy in question.

M_s = the atomic weight of solute.

$R = 8.32 \times 10^7$ ergs/^oK.

$T = 1173^oK$

The molar volume, V_m, of γ' is based on the stoichiometric $Ni_3(Al,Ti)$ unit cell. Since the unit cell can be considered as a molecule, there is one molecule/unit cell, and $V_m = N_o a^3$, where N_o is Avogadro's number, and a is the lattice parameter of the unit cell, 3.58 Å. $V_m = 27.58$ cm^3/mole. An expression for D can be obtained by substituting the above parameters into the equation for k.

$$D = \frac{(9)(1.63\times10^{-21})(8.32\times10^{7})(1173)}{(8)(30)(27.58)^2 c_o}$$

Unfortunately, it is difficult to determine the value of c_o for Nimonic 90, because the phase diagram for this multi-component alloy has not been wholly determined. Accurate evaluation of W_o is, therefore, difficult to accomplish. However, an estimation of this value has been attempted, and details of this estimation follow. Mitchell[18] has determined that the weight-percent of γ' in Nimonic 90 at 700°C is about 20%. Since γ' dissolves at about 950°C, it is estimated that the weight-percent of γ' at 900°C will be about 5%. The total Al + Ti content in the alloy equals about 4w/o, with twice as much Ti as Al. The total concentration of solute in the γ' particles at 900°C, therefore, equals about 1w/o, thus leaving about 3w/o of solute in the matrix γ phase. Thus, $w_o = 0.03$. The density of the matrix phase was calculated from the densities of Ni, Co and Cr, since these elements are

the only predominant constituents in the matrix. By multiplying the densities of the three elements by their ratios in the alloy, a density of 8.11 gms/cm^3 was determined. The same procedure was used to calculate the atomic weight of solute. Since there are twice as many Ti atoms as Al atoms in the alloy, the atomic weight of solute is (0.67) M_{Ti} + (0.33)M_{Al}, which equals 41. Therefore, since $c_o = \rho_X W_o / M_x$,

$$c_o = (8.11)(0.03)/41 = 5.94 \times 10^{-3} \text{moles/cm}^3$$

By substituting the values for the above parameters into the equation $D = 9kRT/8\gamma c_o V_m^2$,

$$D_{calc} = 1.126 \times 10^{-12} \text{sec/cm}^2$$

The diffusion coefficient for aluminum in nickel at 900°C was calculated from the expression $D_{Al} = 1.1\exp(-59{,}500/RT)$ [19] and the diffusion coefficient for titanium in nickel at 900°C was calculated from the expression $D_{Ti} = 1.5\exp(-62{,}800/RT)$ [19]. Therefore,

$$D_{Al} = 8.2 \times 10^{-12} \text{sec/cm}^2 \text{ at } 900^\circ\text{C}$$

$$D_{Ti} = 1.57 \times 10^{-12} \text{sec/cm}^2 \text{ at } 900^\circ\text{C}$$

Since the diffusion of titanium is slower than that of aluminum it would appear that the diffusion of titanium atoms is the rate-controlling step in the growth process. The values of D_{calc} and D_{Ti} are almost identical. This indicates that the assumption that the γ' particles coarsened by a diffusion-controlled mechanism in the soaked specimen of Nimonic 90 is valid.

The relationship between r^3 and t for thermal fatigue is not linear. Thus, Ostwald ripening cannot be the sole mechanism for γ' coarsening during thermal fatigue.

From the limited data obtained in this research, it appears that the γ' particles coarsen by a diffusion-controlled mechanism during aging, but deviate from this manner of growth during thermal fatigue. However, there is much scope for further research into this aspect of the physical metallurgy of nickel-based alloys.

Hardness measurements were taken on the thermally cycled specimens. After an initial drop in hardness which could be accounted for by reversion (the initial aging temperature was 700°C and the maximum cycle temperature 900°C), there was a slight increase in hardness from 230 to 265 VHN. In view of the growth of the γ' particles a softening might be expected, but it would appear that this is counteracted by the work-hardening as a result of the increasing dislocation density.

In addition to the rapid growth of the γ' particles, two other structural changes were observed in Nimonic 90, with increased cycling. (1) carbide precipitation on dislocations and (2) the formation of precipitate free regions adjacent to grain boundaries.

Small spherical particles of $M_{23}C_6$ have formed in areas of high dislocation density after 50 cycles (Fig. 11). Figure 11b is a dark field micrograph taken from one of the $M_{23}C_6$ diffraction spots and shows the location of the carbide particles.

The precipitates are present near the massive carbides due to the high dislocation density associated with these massive particles, which provide ready nucleation sites for the formation of $M_{23}C_6$. Since there is a close structural relationship between the complex f.c.c. structure of the carbide and that of the f.c.c. matrix, and because the lattice parameter of the carbide (A_o = 10.64 Å) is almost exactly three times that of the matrix (A_o = 3.57 Å), it is reasoned that the early stages of precipitation of the $M_{23}C_6$ would produce a coherent precipitate. Merrick[13] observed contrast effects around very small particles of $M_{23}C_6$ in nickel-based alloys which resembled the elastic strain fields around coherent particles. Nucleation on dislocations in the matrix can help to relieve the coherency strain field associated with the small carbide particles and thus dislocations would be favorable carbide nucleation sites. The same is true after 1500 cycles as seen in Fig. 12. A high dislocation density is found near the boundaries of the large carbide particles, since these are very effective barriers to dislocation movement. Carbides have nucleated on these dislocations and the γ' density is lower in this region since chromium is taken out of solution during the carbide precipitation. The effect of chromium on the γ' precipitation will be discussed later.

Dislocations can be observed at the interfaces of these newly formed carbides. Considerable deformation of the massive carbide has been produced by the high numbers of thermal cycles, as indicated by the high dislocation density within the particle.

The incoherent twin boundaries are also favorable carbide nucleation sites.

After 20 cycles, grain boundary migration occurred within precipitate-free regions (Figure 13). Because precipitate-free regions are not formed in Nimonic 90 after aging at 700°C, it must be concluded that the thermal fatigue process produces these large regions. During the high temperature segment of the thermal cycle, the boundaries may migrate through these regions. The boundary in Figure 13 appears to have broken away from the carbide particles which originally formed on it, and to have moved through the precipitate-free region. Note that the precipitate-free region is only on one side of the boundary.

Severe grain boundary denudation has also been observed after 500 thermal cycles, as shown in Figures 14 and 15. Again, the precipitate-free region exists only on one side of the grain boundary. Figure 15

shows a boundary which has migrated during thermal fatigue and dragged some dislocations along with it. The row of carbides appears to have formed on the boundary before migration, but during thermal fatigue the boundary has migrated within the small γ'-free region adjacent to it. Some dislocations appear to exist at the interface between these carbides and the matrix.

A γ'-free region exists adjacent to both sides of the grain boundaries in Fig. 16, due to the growth of the $M_{23}C_6$ particles at the boundaries after 1500 cycles.

Soaking Experiments

In order to examine further the effect of the high temperature segment of the thermal cycle on both the dislocation morphologies and the nucleation of carbides, specimens of both alloys were deformed in tension at room temperature and soaked at 900°C for varying lengths of time. After each thermal treatment, these specimens were examined at room temperature in the electron microscope. A specimen of Nimonic 75 was plastically strained at room temperature 1.5%, while a specimen of Nimonic 90 was plastically strained 2%; both specimens were then soaked for 5, 10, 20 and 30 minutes and examined after each soaking period.

Nimonic 75

After only 5 min, the dislocations had begun to rearrange themselves into recovery networks. Carbides have precipitated on grain, twin, and sub-boundaries, and also on individual dislocations. Both TiC and M_7C_3 had precipitated out during soaking. As the soaking time was increased, more dislocation rearrangement was observed, and continued nucleation and growth of carbide particles occur.

Nimonic 90

This alloy exhibits a much greater resistance to recovery than Nimonic 75. After a 5 min soak, no sub-boundaries were present, and it was difficult to ascertain whether carbide precipitation had occurred. With longer soaking times, carbide ($M_{23}C_6$) precipitation on slip lines was observed but there was very little evidence of recovery (Fig. 17).

Constrained Specimens (Tapered-Disc Type)

Nimonic 75

With a maximum cycle temperature of 800°C visible cracks were produced after 150 cycles, but testing was continued to a total of 205 cycles. The dislocation morphologies were very similar to those found in the absence of constraint, in that much recovery had taken place, but in this case, the dislocation densities were higher.

Examination of the fractured area by optical microscopy showed that the cracks were predominantly intergranular in nature. This is shown

in Figure 18. Although the grain boundaries are not etched themselves, carbide particles appear to outline the individual grains. Pores appear to have formed on some of the grain boundaries and in some cases they appear to have coalesced.

When the maximum cycle temperature was increased to 900°C, visible cracks occurred after 40 cycles, but the test was continued for a total of 100 cycles. With the higher cycle temperature, extensive recovery had occurred and there was clear evidence for carbide precipitation on recovery networks and at the interfaces of massive particles of TiC (Fig.19).

Nimonic 90

With a maximum cycle temperature of 800°C, cracks first formed after 470 cycles, but testing was continued for 535 cycles. Upon examination of this specimen in the electron microscope, two primary effects were observed. Firstly, most of the dislocations were contained in slip-bands, and secondly, carbides were precipitated on the dislocations. Figure 20, shows dislocations which are confined to the (111) slip planes. This was confirmed by single-surface analysis of the diffraction patterns from these areas. Both loops and super dislocations are present in this micrograph.

Carbide precipitation on dislocations was observed in this specimen. In addition to the precipitation of $M_{23}C_6$ on dislocations, small particles of $M_{23}C_6$ appeared to form on the surfaces of massive particles of TiC. Bilsby[30] has observed the same precipitation phenomenon in creep tested specimens of Nimonic 80A. Some of the foils from this specimen contain cracks along grain boundaries as shown in Figure 21. The crack shown in this micrograph appears to have been produced by chemical attack rather than by a large build-up of thermal stresses. The fact that the crack surfaces are irregular and, in some instances, penetrate between the particles of $M_{23}C_6$ supports this point of view. The preferential etching at grain boundaries during electropolishing may have occurred because of a chromium-depleted region adjacent to the grain boundary carbides. If this is the case, then the γ'-free regions formed during thermal fatigue can be susceptible to preferential chemical attack.

On raising the maximum cycle temperature to 900°C, different dislocation morphologies were produced and fracture was first observed after 50 cycles. The cycling was, however, continued for 100 cycles before the specimen was metallographically examined. Figure 22 shows the arrangement of dislocations near a grain boundary. The dislocations are randomly distributed and irregularly shaped. No dislocation loops or superdislocations are present. The average γ' particle diameter was approximately 540 Å, which is approximately equal to the average γ' particle diameter produced in an unconstrained specimen which was cycled the same number of times. A γ'-free region adjacent to the boundary is present. Carbides are present both at the grain boundary and in regions of high dislocation density within the γ'-free region. Interface dislocations surround some of these particles (at A in Figure 22).

Many well-defined sub-boundary networks have formed in the γ'-free region and these are shown at B in Figure 22. This region shows extensive recovory, probably due to the higher mobility of the dislocations in regions which do not contain any γ' particles.

Within the interior of the grains, the dislocations are either randomly dispersed or contained within slip-bands. This is shown in Figure 23. This figure shows two arrays which contain a high density of dislocations. Trace analysis has indicated that these arrays lie in (111) planes and are therefore slip-bands. Because of the higher testing temperatures, the slip-bands become less well-defined and the dislocations are more randomly dispersed than those found in the specimen tested at a maximum cycle temperature of 800°C. This is due to the fact that many of the dislocations which lay on the slip planes have climbed out of their original configurations under the influence of the high testing temperature. Carbides have formed on the dislocation arrays. These particles were most likely nucleated on the dislocation arrays and grew during the thermal fatigue process. Further evidence for carbide formation on dislocations is shown in Figure 24. These carbides have formed in the vicinity of massive carbide particles which were present before thermal fatigue testing had begun. There appears to be a γ'-free region adjacent to these carbides, and the dislocations within this region have formed into well-defined recovery networks.

The fractured areas of this specimen were also examined optically. All of the fractures initiated at the periphery of the tapered disc, and the cracks were intergranular in nature. This is shown in Figures 25 and 26. Considerable carbide precipitation in some grains very close to the periphery of the disc had occurred. This precipitation appears to have taken place on slip-bands, although more random carbide precipitation is also observed in many of the grains. This can be seen at point A in Figure 25. Carbides are prevalent along almost all of the grain boundaries, and a corrosion product appears to have penetrated the cracks which were initiated at the periphery (point A, Figure 26). The very small grains at or near the surface of the specimen are believed to have formed by recrystallization, since they are situated in regions of maximum temperature and stress. However, identification of this phase was not attempted. The thermal fatigue fractures in both Nimonic 75 and Nimonic 90 bear a great resemblence to the creep fractures reported by Betteridge and Franklin[20], Johnson and Khan[21], McLean[22], and Heslop[23]. It is possible that a creep-type mechanism may be responsible for fracture in these specimens.

It appears that the dislocation morphologies produced in these constrained specimens were similar to the dislocation morphologies produced in the unconstrained specimens which had experienced a large number of thermal cycles. Extensive recovery at both maximum cycle temperatures had taken place in Nimonic 75 as well as carbide precipitation on dislocations. Nimonic 90 showed evidence of recovery only when the maximum cycle temperature was 900°C, and this was not as pronounced as in Nimonic 75 since no actual sub-boundaries formed within the interior of

the grains. γ'-free regions were formed which did, however, contain a large number of well-defined recovery networks. Carbide precipitation was very prevalent in this alloy at both maximum cycle temperatures. The interfaces of the large particles of TiC appear to provide favorable sites for the nucleation of particles of M_7C_3 or $M_{23}C_6$. Since the TiC phase is incoherent with the matrix, there is a large number of dislocations at the interface of the two phases. The dislocation density could be quite high for particles of large size. These dislocations could provide the necessary nuclei for the precipitation of the carbide particles. In effect, the interface between the TiC and the matrix phases is similar to a grain boundary as far as carbide nucleation is concerned. There is enough carbon in solid solution in both alloys to allow the precipitation to take place, and since the TiC does not contain any chromium (the major metallic element in both M_7C_3 and $M_{23}C_6$), there will not be a chromium-depleted region adjacent to the TiC which could prevent the formation of the chromium-rich carbides.

DISCUSSION

It would appear that, during thermal cycling of unconstrained specimens, dislocations are generated chiefly by a prismatic punching mechanism from dispersed phases. It is probable that some dislocations are also generated at twin and grain boundaries. For constrained specimens, it is likely that prismatic punching plays a lesser role in dislocation generation since considerable thermal strains are produced because the specimens are prevented from freely expanding and contracting.

The dislocation morphologies are greatly influenced by the total plastic strain, maximum cycle temperature, and the total time the specmen remains at the elevated temperatures. All of these are directly related to the total number of thermal cycles the specimens experience. This means that during thermal fatigue, as the deformation and total time spent at the high temperatures increases, recovery takes place, causing a rearrangement of the dislocations. Recovery is easily accomplished in Nimonic 75, as evidenced by the large numbers of well-defined sub-boundaries and randomly dispersed dislocations. Nimonic 90, on the other hand, resists recovery to a much higher degree than Nimonic 75. Less well-delineated sub-boundaries are formed after a large number of cycles, and slip lines are still present. The presence of γ' particles evidently hinders the movement of the dislocations, thus making it more difficult to form recovery networks. Additional information regarding the relationship between dislocation morphology and the duration of time a specimen spends at elevated temperatures is obtained from a study of the micrographs taken of specimens plastically deformed at room temperature and soaked at 900°C for various periods of time. Nimonic 75 shows substantial recovery after only short soaking times. Nimonic 90 again shows a resistance to recovery; the dislocations remain in their slip planes, although these become less well-defined the longer the specimen is soaked. In both alloys, carbide precipitation on dislocations is very prevalent.

The dislocation morphologies produced by the thermal fatigue of unconstrained, and tapered-disc specimens appears to be similar. However, the dislocation density was higher and recovery occurred after few cycles for the constrained specimens. Thus, the imposition of constraints will result in shorter lifetimes, but will not alter the nature of the thermal fatigue damage.

The dislocation morphology in Nimonic 90 is also influenced by the dispersion of the γ' phase in the alloy. This dispersion is in turn influenced by the testing times and temperatures. The γ' particle diameter increases with increasing numbers of thermal fatigue cycles. The growth is, however, faster in the early stages than when the specimen was simply aged for an equivalent period of time at the maximum cycle temperature. This means that the change in the distribution of secondary phases with increased testing cannot be predicted from aging data alone.

In the early stages of the thermal fatigue of Nimonic 90, the γ' particle size is quite small; thus, superlattice dislocations are produced during plastic deformation because of the shearing of the γ' particles. As testing is continued, the γ' particle diameter rapidly increases to a size where dislocations can no longer shear some of the particles, but must circumvent them by either bowing between them or cross-slipping around them, thus leaving prismatic loops around the γ' particles. Upon further testing, the γ' particle size and interparticle spacing become so large that the dislocations can more easily pass between the particles without always having to resort to bending between them. The high temperatures involved in the testing provide the dislocations with high mobility since the process of climb is then relatively easy to accomplish. Thus, as well as producing thermal strains, the testing temperatures influence the behavior of the alloys by influencing the movement of dislocations through the lattice.

Age-hardenable nickel-based alloys are selected for use as turbine blading because of their combined good high temperature strength and creep resistance. These superior mechanical properties at high temperatures arise from the fact that the γ' phase grows only very slowly, thus allowing the alloys to maintain high strengths after long periods of time at high temperatures. However, because thermal cycling causes Nimonic 90 to overage more rapidly than would be expected, the strength of this alloy would decrease more rapidly. This means that, apart from the direct damage created by the thermal fatigue process, thermal fatigue may cause materials to be more susceptible to failure by other mechanisms. This may explain why many thermal fatigue fractures closely resemble creep fractures in that, with both types of failure, the specimens appear to show a susceptibility to grain boundary fracture.

There is no doubt that recovery can occur during the high temperature segment of the thermal cycle. This is especially evident in Nimonic 75. Nimonic 90 appears to resist recovery to a much greater

extent than Nimonic 75, most probably because of the presence of γ' particles which hinder dislocation movement. If recovery does occur it may well prevent excessive work hardening and give improved resistance to fracture. Davies, Dennison and Evans[24] have shown that the annealing creep tested specimens of Nimonic 80A recovery occurred, thus prolonging the creep lives of the specimens. The recovery phenomenon may explain the data of Glenny and Taylor[2] where at high maximum cycle temperatures the thermal fatigue life of Nimonic 75 is almost the same as that of the high strength age-hardenable alloys. At these high temperatures, where ductility is very important, a large amount of recovery occurred in Nimonic 75, but much less in the more sophisticated alloys. Thus, Nimonic 75 is more ductile and this may more than compensate for its lower strength. Glenny and Taylor also reported that above a critical maximum cycle temperature the thermal endurances of all the Nimonic alloys improve. This can also be explained by the fact that above this critical temperature (which varies according to the alloy) a large amount of recovery may take place, thus increasing the ductility of these alloys. It is accepted that increasing the ductility will give rise to improved thermal endurance and it seems likely that high temperature ductility and the ability to recover are closely associated.

Thermally cycled specimens of Nimonic 90 exhibited precipitate-free regions adjacent to grain boundaries. In many cases these regions were situated on only one side of the boundary and since they were never observed in the heat treated specimens, it is concluded that the precipitate-free regions from during thermal cycling. A possible explanation for the formation of these γ'-free regions follows. Cellular precipitation of $M_{23}C_6$ occurs during aging (Figure 6). Within the region containing the cellular carbides, no γ' particles are nucleated owing to the low chromium concentration in the matrix material that exists between the carbide rods. The loss of chromium is thought to increase the solubility for titanium and aluminum of the matrix, thus retarding the formation of the γ' phase. During the high temperature segment of the thermal fatigue cycle, the carbide particles may spheroidize and grow, thus maintaining the low chromium concentration on one side of the boundary; the γ' particles would still be prevented from forming in this region. In some cases the grain boundary appears to have moved within the precipitate-free region, thus freeing itself from the carbides. It is much easier for a grain boundary to move within such a region than to move in a region containing coherent particles. For the boundary to migrate in a region containing γ' particles, the particles would have to dissolve, since otherwise, they would no longer be coherent with the new grain. In some cases the boundary had broken away from the carbides which had formed on it. This means that the boundary is no longer anchored by the carbides and would be more susceptible to cavitation. The boundary could "open up" if fracture were initiated on it since there would be no carbides there to prevent further movement of the crack. Also, since the boundary is now mobile, grain boundary sliding may more easily occur.

The removal of chromium from the grain boundary regions by the growth of the carbides may make the boundaries susceptible to crack

initiation since the corrosion resistance in these regions is reduced. This would be more pronounced the higher the maximum cycle temperature. Oxide penetration along grain boundaries was observed by Glenny and Taylor and they postulated that preferential oxidation of this type could lead to a lowering of the thermal endurance. What appears to be oxide penetration along grain boundaries was also observed in the fractured specimens examined in this work. If the grain boundary areas become susceptible to oxidation during the thermal fatigue process, especially at very high temperatures, this may help to explain why thermal fatigue fractures are transgranular at low maximum temperatures but become intergranular at high maximum cycle temperatures. There can be no doubt that oxidation influence thermal endurance; this was clearly demonstrated by Glenny and Taylor. However, a great deal more work is necessary in order to determine accurately the degree to which the γ'-free regions are susceptible to oxidation.

Thermal cycling has the effect of altering the microstructure of Nimonic 90 by causing a coarsening of the γ' precipitate particles, and by altering the distribution of these particles near grain boundaries. A third major alteration in microstructure is also observed which occurs in both Nimonic 75 and Nimonic 90. Carbide precipitation on dislocations generated during thermal fatigue occurs throughout the grains of both alloys, producing a change in the distribution of these phases from that originally determined by the heat treatment conditions. Betteridge and Franklin[20] have examined the effect of heat treatment and structure on the creep and stress-rupture properties of Nimonic 80A. They found that the creep and stress-rupture properties of the alloy were optimum when solution-treatment was carried out at 1080°C; lower temperatures led to higher creep rates, and high temperatures caused early rupture at small values of creep strain. This behavior was found to be directly related to the manner of precipitation of chromium carbide within the alloy. High solution-treatment temperatures (1150°C) produced very little carbide at the grain boundaries; most of this phase was randomly distributed throughout the grains. This, in turn, caused early fracture with very little extension, even though the creep rate was low. The best life-to-fracture was obtained after treatments which produced a fairly uniformly distributed chain of chromium-rich carbide particles along the grain boundaries. The authors reasoned that the effect of the precipitation of carbide was to produce, around the boundaries, zones which were impoverished in chromium and therefore reduced in strength. These zones would permit the relaxation of stresses which concentrate at the grain boundaries, thus prolonging life by delaying fracture.

Duce, Hicks and Potter[25] have noted that heat treatments which gave the best creep ductilities were also best from the point of view of thermal fatigue endurance. The best creep properties occurred when carbides were precipitated at grain boundaries, producing a region depleted in γ' adjacent to the boundary. However, in some cases failure at low elongations occurred. It was suggested that strengthening of the matrix occurred during testing due to general precipitation of carbides

within the grains, thus throwing much of the strain onto the grain boundary denuded regions. This, together with a rigid boundary, was thought to be the reason for the poor properties observed. The denuded regions adjacent to the grain boundaries can have beneficial properties if the grains do not become too strengthened. However, these regions may have deleterious properties if the grains become too hard. Numerous workers[26,27] have reported grain boundary fracture in heat-affected zones of welds in fully austenitic steels, caused by strain-induced precipitation of carbides which give rise to low ductilities, throwing the strain onto the grain boundary regions. Irvin, et al.[28] mechanically tested an austenitic stainless steel at temperatures between 550°C and 700°C. They found that small particles of NbC had precipitated on dislocations at these temperatures. This stress-induced precipitation produced intergranular fracture and a marked loss of ductility. They reasoned that the precipitation process increased the high temperature strength of the grains, causing much of the deformation to be thrown onto the grain boundaries. This process was accentuated by the presence of grain boundary denuded regions which are weak compared with the matrix, although their presence is not necessary for this process to take place.

Examination by optical microscopy of unconstrained specimens of Nimonic 90 which have undergone 10, 20 and 50 thermal cycles, respectively was attempted. A comparison of these microstructures with that present before thermal cycling indicates that thermal cycling increases the number of carbide particles present both at grain boundaries and within the grains.

Carbide precipitation on dislocations within the grains of both Nimonic 75 and Nimonic 90 may have a serious embrittling effect upon the materials. It could lead to enhanced creep resistance of the grains and a consequent transfer of strain to the weakened grain boundary regions. This, together with a decreased oxidation resistance at the boundaries, could explain why thermally fatigued nickel-based alloys show susceptibility to intergranular fracture. The strain-induced precipitation of carbides at elevated temperatures may explain why Franklin, et al.[8] observed a ductility minimum at 800°C to 900°C for all of the γ'-hardened alloys tested.

It is obvious that the distribution of carbide phases greatly influences the high temperature mechanical properties of the alloys. The most desirable properties result when the carbides are situated at the grain boundaries and are not distributed throughout the grains. Therefore, any process which tends to redistribute these carbides, producing a less desirable dispersion, will cause a shortening in the lives of the alloys. The thermal fatigue process involving high maximum cycle temperatures ($\geq$ 800°C) appears to alter the distribution of carbides within both Nimonic 75 and Nimonic 90. In the past, the compositions and heat treatments of nickel-based alloys were manipulated in order to produce optimum high temperature tensile and creep properties. Since thermal fatigue is a major cause of failure in fluctuating temperature

environments, this mode of thinking may have to be altered. Although the presence of carbon may improve the creep ductility of Nimonic alloys, it would appear from the present investigation that the presence of carbon either in the form of massive carbides or as fine carbides on dislocations can be deleterious. Therefore, a compromise in composition and heat treatment may have to be devised so as to produce an optimum combination of high temperature thermal fatigue, and creep properties. This may be accomplished by lowering the carbon content of these alloys and introducing an intermediate heat treatment in order to take all the carbon out of solution in the form of grain boundary carbides, leaving no free carbon to form precipitates on dislocations during testing. An alternative would be to develop new techniques for improving creep ductility other than by the addition of carbon to the nickel-based superalloys.

In general, this investigation has made it clear that, during the thermal fatigue of complex alloys, the microstructural constituents are very influential in thermal endurance. Large carbide particles provide a source for dislocation generation. These particles also affect the ductility and strength of these alloys. The distribution of these phases changes during testing, producing a corresponding change in mechanical properties. The thermal fatigue process also affects the size and distribution of any age-hardening phase which may be present in the alloys. Rapid overaging can occur and precipitate-free regions can be produced during thermal fatigue. The age-hardening phase influences the movement of dislocations which, in turn, influences mechanical properties. The changes in microstructure produced by thermal fatigue tend to produce less favorable mechanical properties as testing is continued. Thus it appears that the findings of Forrest and Armstrong[6,7] and Franklin et al.[8]. that the thermal fatigue resistance of a material is dependent upon a combination of strength and ductility throughout the whole temperature range of application, are largely substantiated by the present investigations.

CONCLUSIONS

1. The dispersed carbide phases in both alloys appear to be responsible for dislocation generation by prismatic punching during thermal fatigue. These particles also provide barriers for dislocation movement, thus producing an accumulation of dislocations in regions of the matrix adjacent to them.

2. The thermal fatigue process causes an accelerated growth of the γ' particles in the Nimonic 90 specimens up to a particle diameter of about 500 Å. Above this value, the precipitate particles appear to grow at about the same rate in thermal fatigue as in soaking at 900°C. The γ' particle diameter is influential in determining the dislocation morphology produced by thermal fatigue. When the γ' particles are small, superlattice dislocations are produced due to the shearing of the γ' particles. For larger γ' diameters, prismatic loops are formed around the γ' particles since it is now

easier for a dislocation to bow between the precipitate particles than to shear them. For the large γ' diameters and large interparticle spacings, the dislocations can easily circumvent the precipitates and thus very few loops are formed. Also, loose subboundary arrays can form since the γ' particles do not now constitute much of a barrier to dislocation movement.

3. Carbide precipitation on dislocations occurs during thermal cycling. The resulting increase in the number of carbide particles most likely causes a strengthening of the grains and a consequent loss of ductility. This will be more pronounced in constrained thermal fatigue specimens since the dislocation densities are high, and, in the case of Nimonic 90, failure will probably occur before the alloy overages sufficiently to counterbalance the embrittlement caused by the presence of the carbides.

4. The precipitate-free regions, usually adjacent to one side of the grain boundaries, which were sometimes observed in thermally fatigued specimens of Nimonic 90, are thought to have formed by cellular precipitation. A chromium-depleted region is maintained in the area which contained the cellular carbides, thus preventing the formation of any γ' particles. Some grain boundary migration within this region was also observed. It is thought that the presence of these regions makes the alloy more susceptible to grain boundary fracture for two reasons. Firstly, preferential corrosion can occur in these regions since they contain a lower chromium concentration than the rest of the alloy. Secondly, these regions are weaker than the interior of the grains and less able to withstand high stresses, especially if there is a high stress concentration in the depleted regions caused by the carbide-strengthened grain interiors. These regions can be beneficial to creep resistance since the relaxation of thermal stress can occur near grain boundaries. However, if too many of the thermal stresses become concentrated in these regions because of the highly strengthened grain interiors, these softer regions will then be undesirable. It thus appears that although the original microstructures of these alloys may be desirable, the thermal fatigue process produces microstructural changes which are highly undesirable.

5. Nimonic 75 shows a great tendency for recovery at elevated temperatures. Thus, even after large thermal strains, this alloy will remain quite ductile, which is important at elevated temperatures. Nimonic 90, on the other hand, shows a great resistance to recovery and this may explain why the thermal endurances of the two alloys become almost identical at high maximum cycle temperatures where ductility appears to be the most important mechanical property.

FUTURE WORK

It would be desirable to thermally fatigue both constrained and unconstrained specimens of Nimonic 75 and Nimonic 90 with varying carbon compositions and carbide distributions. In this way, a more tangible relationship between the distribution of carbides and thermal fatigue life could be obtained. The influence of corrosion on thermal endurance is as yet not fully determined. Other than the fact that corrosion reduces thermal endurance, little is known about the mechanism. Tests should be carried out in order to see if corrosion does indeed start crack initiation at grain boundaries and if the γ'-depleted regions do initiate grain boundary oxidation. The distribution of γ' appears to indluence recovery in these alloys. It may prove fruitful to investigate the relationship between γ' interparticle spacing and recovery. Other high temperature alloys should be thermally fatigued in order to determine whether the results of this research can be applied to other systems. In this way, more general relationships between thermal fatigue failure and materials can be obtained.

ACKNOWLEDGMENTS

The authors would like to thank Dr. W. I. Mitchell of the International Nickel Co., Ltd. Research Laboratories, Birmingham, for carrying out the thermal fatigue tests on the NGTE specimens; Mr. M. Morley of Henry Wiggin and Co., Letc. for help in the spark machining of disc from these specimens. Acknowledgment is made to the Ministry of Technology for supporting this work.

REFERENCES

1. E. Glenny, J. E. Northwood, S. W. K. Shaw and T. A. Taylor, J. Inst. Metals, Vol. 87, 1958-59, p. 294.

2. E. Glenny and T. A. Taylor, J. Inst. Metals, Vol. 88, 1959-60, p. 449.

3. E. Glenny, Met. Reviews, Vol. 6, No. 24, 1961, p. 387.

4. H. G. Baron and B. S. Bloomfield, J. Iron and Steel Inst., Vol. 197, March 1961, p. 223.

5. F. J. Clauss and J. W. Freeman, NACA TN-4160, Sept., 1958.

6. P. G. Forrest and K. B. Armstrong, "Joint International Conference on Creep", 1963, Book 2, Paper 1, Session 3, p. 1, London.

7. P. G. Forrest and K. B. Armstrong, J. Inst. Metals, Vol. 94, 1966, p. 204.

8. A. W. Franklin, J. Heslop, and R. A. Smith, J. Inst. Metals, Vol. 92, 1963-64, p. 313.

9. G. W. Briers, D. W. Dawe, M. A. P. Dewey, and I. S. Brammor, J. Inst. of Metals, Vol. 93, Nov., 1964, p. 77.

10. P. C. Becker and J. Nutting, Proc. Int. Conf. on Thermal and High-Strain Fatigue, June, 1967, London, p. 100.

11. M. J. Marcinkowski, "Electron Microscopy and Strength of Crystals", (J. Wiley and Sons, N.Y.), 1963, p. 333.

12. E. Orowan, "Symposium on Internal Stresses in Metals and Alloys", J. Inst. Metals, 1948, discussion, p. 451.

13. H. F. Merrick, Ph.D. Thesis, Univ. of Cambridge, 1963.

14. R. A. Oriani, Acta Met., Vol. 12, 1964, p. 1399.

15. A. J. Ardell and R. B. Nicholson, J. Phys. Chem. Solids, Vol. 27, 1966, p. 1793.

16. C. Wagner, Z. Electrochem., Vol. 65, 1961, p. 581.

17. W. I. Mitchell, Z. Metal., Vol. 57, 1966, p. 586.

18. W. I. Mitchell - Private Communication.

19. Y. Adda and J. Philibert, "LaDiffusion Daus Les Solides", Vol. II, (Presses Universitaires De France), 1966.

20. W. Betteridge and A. W. Franklin, J. Inst. Metals, Vol. 85, 1956-57, p. 473.

21. A. E. Johnson and B. Khan, Metallurgia, Vol. 72, Aug., 1965, p. 55.

22. D. McLean, J. Inst. of Metals, Vol. 85, 1956-57, p. 468.

23. J. Heslop, J. Inst. of Metals, Vol. 91, 1962-63, p. 28.

24. P. W. Davies, J. P. Dennison, H. E. Evans, J. Inst. of Metals, Vol. 94, 1966, p. 276.

25. A. G. Duce, B. Hicks, and W. A. Potter, "Joint International Conference on Creep", 1963, Book 4, Paper 59, Session 5, p. 43, London (Inst. Mech. Eng.)

26. J. Truman and H. W. Kirkby, J. Iron and Steel Inst., Vol. 196, Oct., 1960, p. 180.

27. R. N. Younger and R. G. Baker, J. Iron and Steel Inst., Vol. 196, Oct., 1960.

28. K. J. Irvine, J. D. Murray and F. B. Pickering, J. Iron and Steel Inst., Vol. 196, Oct., 1960, p. 166.

29. D. A. Jones and J. W. Mitchell, Phil. Mag., Vol. 3, 1958, p. 1.

30. C. F. Bilsby, Conference on Electron Microscopy, 1966, Manchester, England (Unpublished).

TABLE I

COMPOSITION (WT.%) AND HEAT TREATMENT OF NIMONIC ALLOYS

Heat Treatment	C	Si	Fe	Mn	Cr	Ti	Al	Co	B	Zr	Mg
Nimonic 75											
1/2 hr at 1080° A.C.	0.12	0.06	3	0.25	19.9	0.57	0.29	0.5	0.001	0.02	0.002
Nimonic 90											
8 hr at 1080°C A.C. 16 hr at 700°C A.C.	0.095	0.079	0.9	0.05	18.9	2.53	1.55	15.6	0.003	0.05	0.001

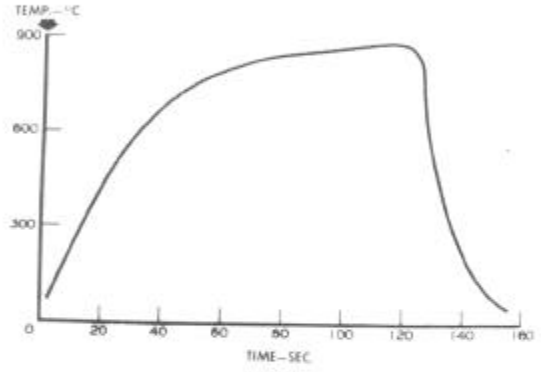

Fig.1. Schematic diagram of the thermal fatigue cycle.

Fig.2. Nimonic 75, 8 thermal cycles, showing the prismatic punching of dislocations from around a particle of M_7C_3. X35,000

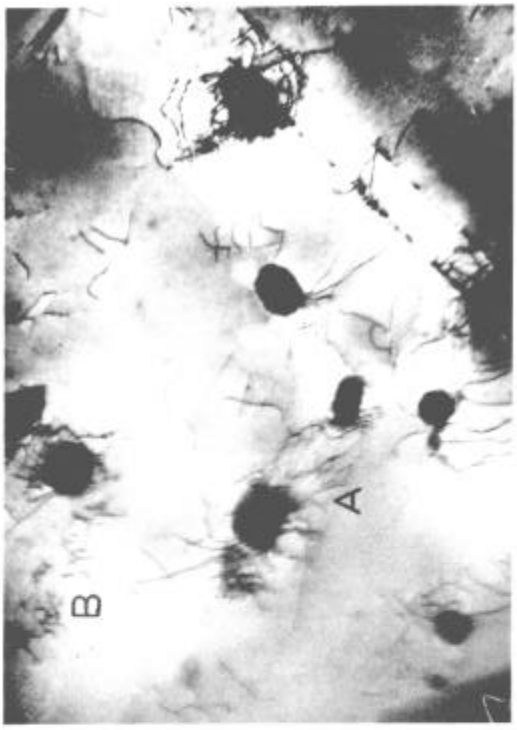

Fig.3. Nimonic 75, 50 thermal cycles. Evidences of recovery are shown at A and B. X20,000

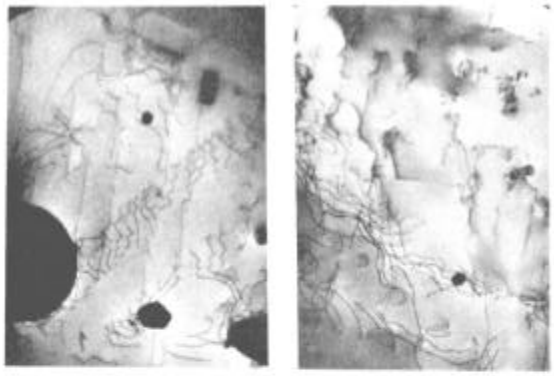

Fig.4. Nimonic 75, 100 thermal cycles. Formation of rudementary recovery networks. X10,000

Fig.5. Nimonic 75, 1500 thermal cycles. Note well defined recovery networks. X17,500

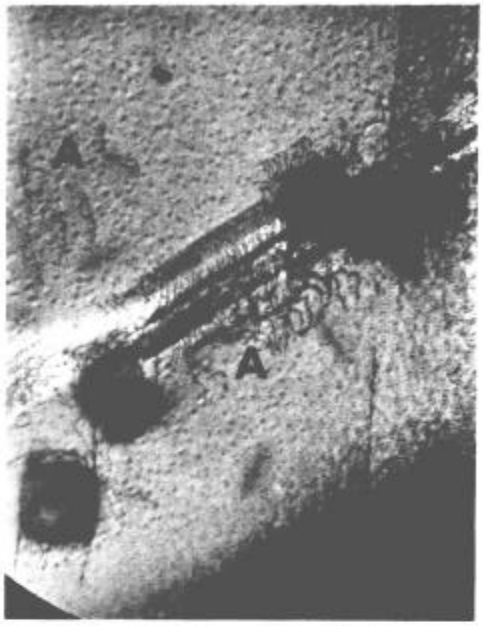

Fig.7. Nimonic 90, 10 thermal cycles. Note superlattice dislocations at A. X17,500

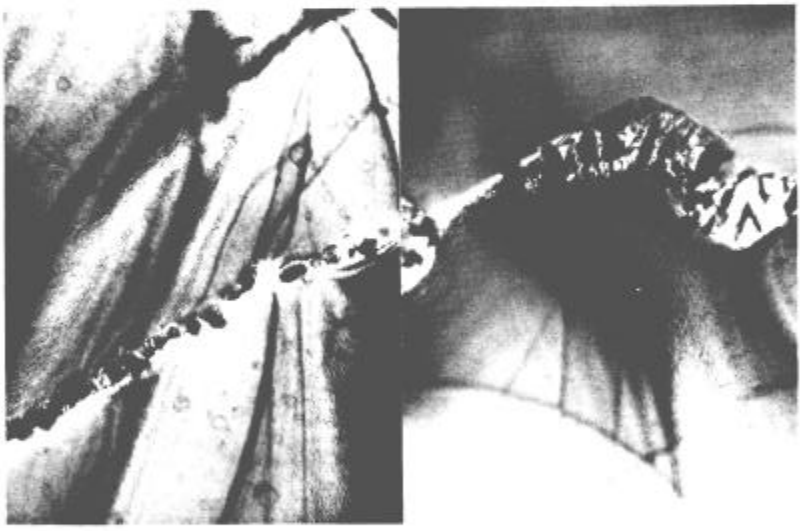

a b

Fig.6. Nimonic 90, commercial heat-treatment and zero thermal cycles. a) Heterogeneous nucleation of $M_{23}C_6$ at grain boundary. b) Cellular precipitation of $M_{23}C_6$. X15,000

Fig.8. Nimonic 90, 250 thermal cycles showing loose tangle of dislocations outlining a sub-grain. X17,500

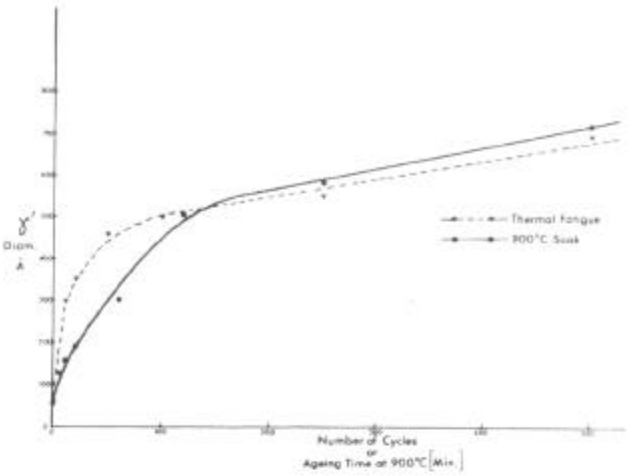

Fig.9. γ' diameter (Å) vs No. of thermal cycles (20°C to 900°C) or aging time (min.) at 900°C.

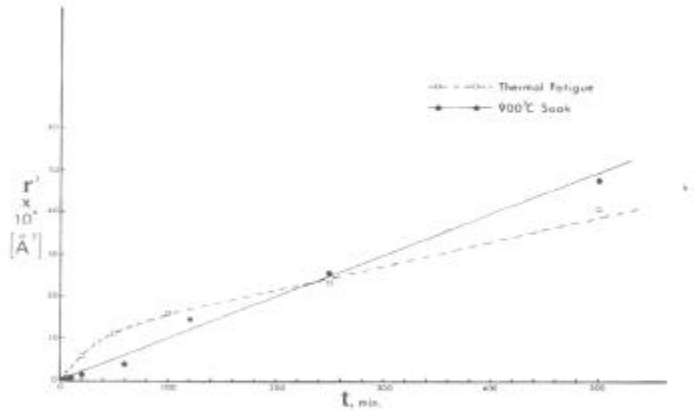

Fig.10. $\bar{r}^3$ vs t, for both the 900°C soaked and the thermally fatigued specimens.

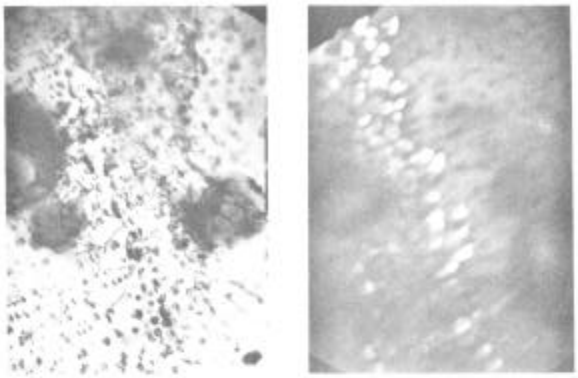

a b

Fig.11. Nimonic 90, 50 thermal cycles. a) Bright field. b) Dark field micrograph from a $M_{23}C_6$ diffraction spot. X15,000

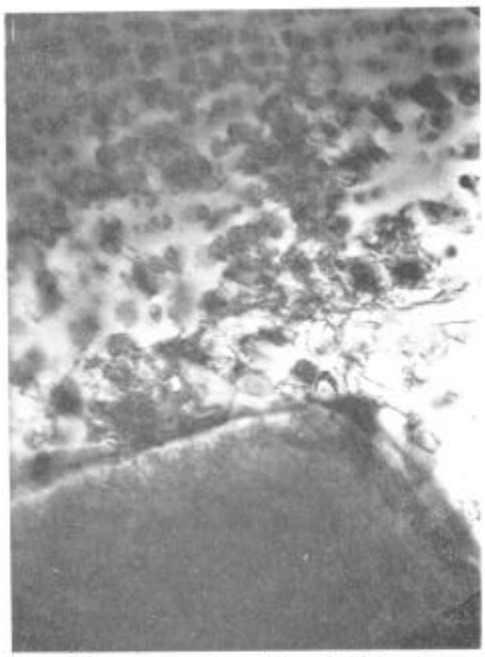

Fig.12. Nimonic 90, 1500 thermal cycles showing $M_{23}C_6$ particles which have nucleated on dislocations near a massive particle of TiC. X25,000

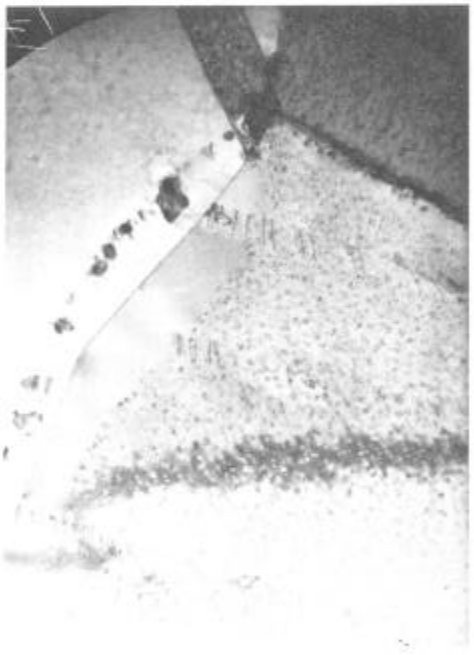

Fig.13. Nimonic 90, 20 thermal cycles, showing a γ'-free region at a grain boundary. Note that the boundary has moved into this region. X17,500

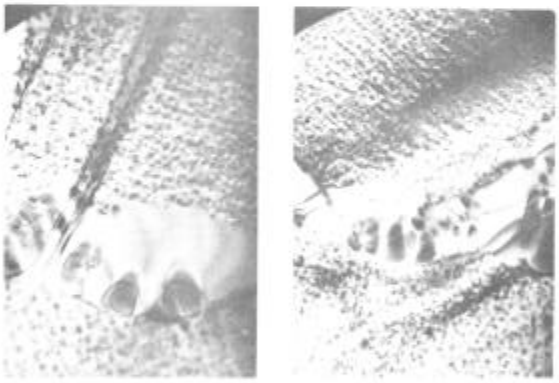

Fig.14. Nimonic 90, 500 thermal cycles showing γ'-free regions adjacent to only one side of grain boundaries. X11,500

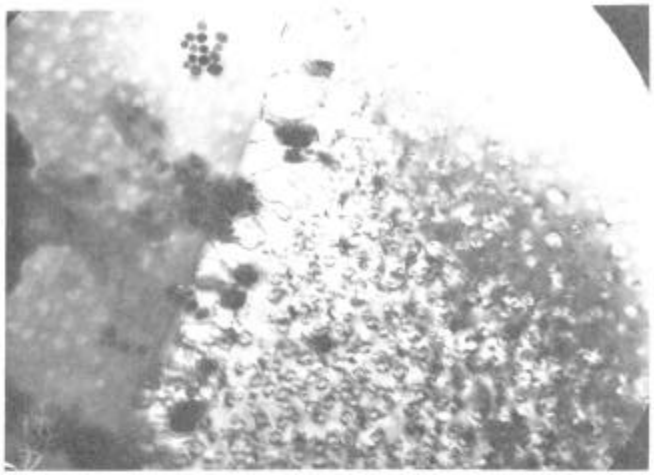

Fig.15. Nimonic 90, 500 thermal cycles showing γ'-free region adjacent to grain boundary. X17,500

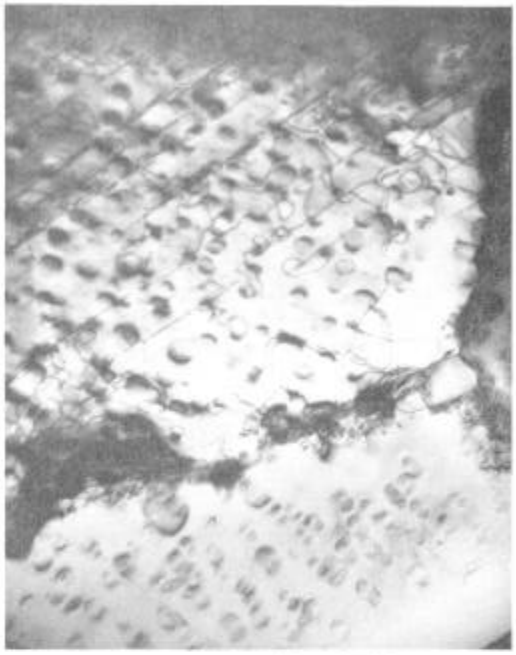

Fig.16. Nimonic 90, 1500 thermal cycles showing γ'-free regions adjacent to both sides of a grain boundary. X12,500

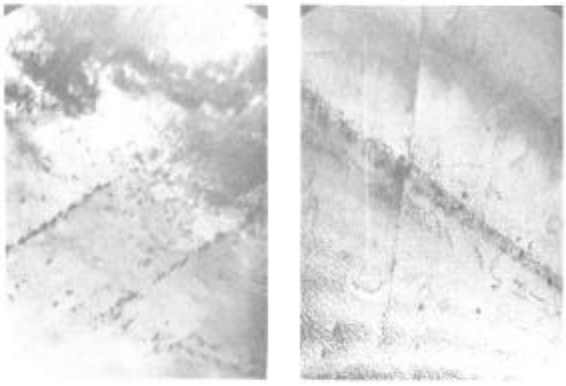

Fig.17. Nimonic 90, 2% plastic strain at room temperature + 20 min. soak at 900°C. Dislocation arrays are on the {111} slip planes. X12,000

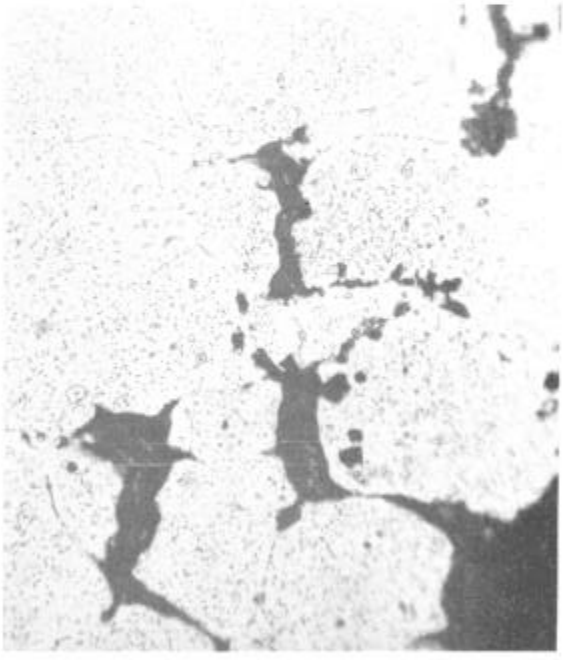

Fig.18. Nimonic 75, optical micrograph of the edge of a tapered-disc specimen. The specimen experienced 205 thermal cycles with a maximum cycle temperature of 800°C. Fracture was first observed after 150 cycles. 400X

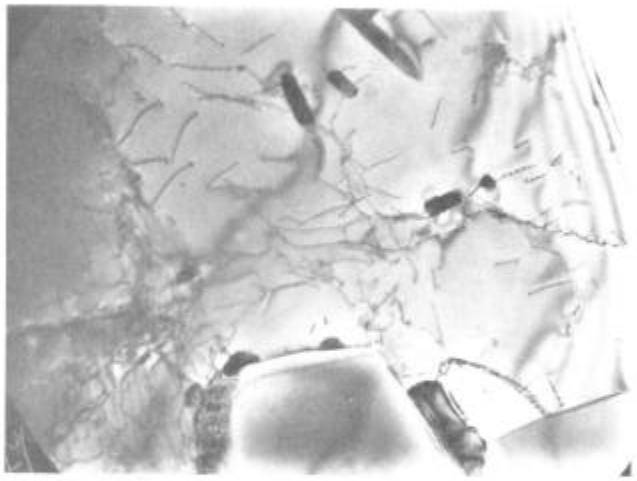

Fig.19. Nimonic 75, constrained specimen thermally fatigued for 100 cycles with a maximum cycle temperature of 900°C. Fracture was first observed after 40 cycles. X16,000

Fig.20. Nimonic 90, constrained specimen thermally fatigued for 535 cycles at a maximum cycle temperature of 800°C. Fracture was first observed after 470 cycles. X16,000

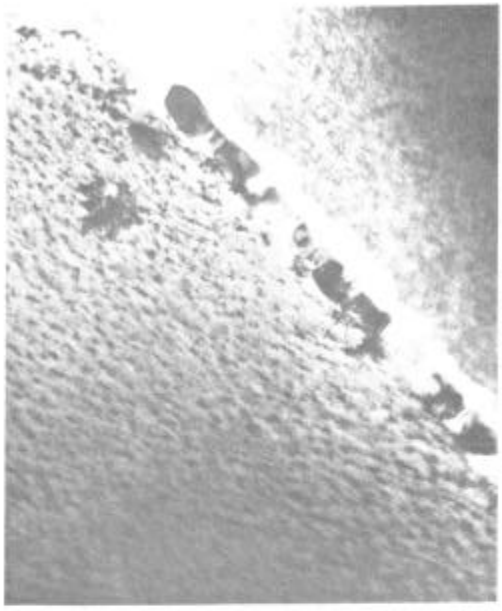

Fig.21. Nimonic 90, constrained specimen thermally fatigued for 535 cycles at a maximum cycle temperature of 800°C. Fracture was first observed after 470 cycles. X16,000

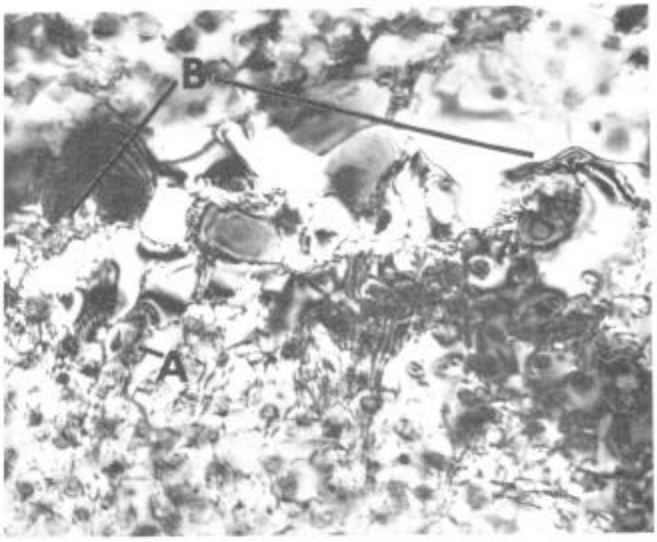

Fig.22. Nimonic 90, constrained specimen thermally cycled for 100 cycles at a maximum cycle temperature of 900°C. Fracture was first observed after 50 cycles. Interface dislocations around particles of $M_{23}C_6$ are shown at A, while sub-boundary networks are at B. X51,000

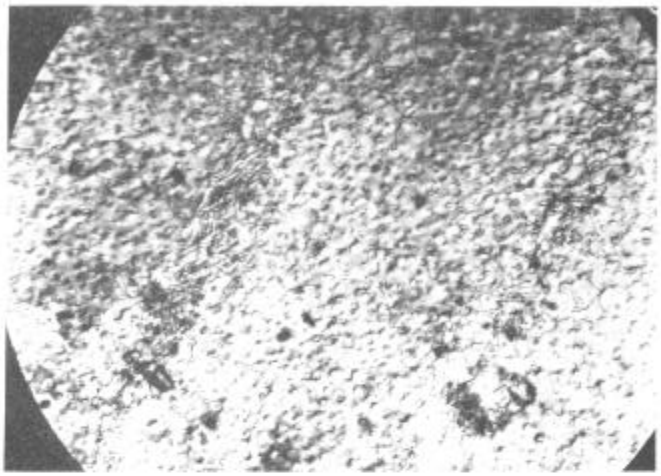

Fig.23. Nimonic 90, constrained specimen thermally cycled for 100 cycles at a maximum cycle temperature of 900°C. Fracture was first observed after 50 cycles. X16,000

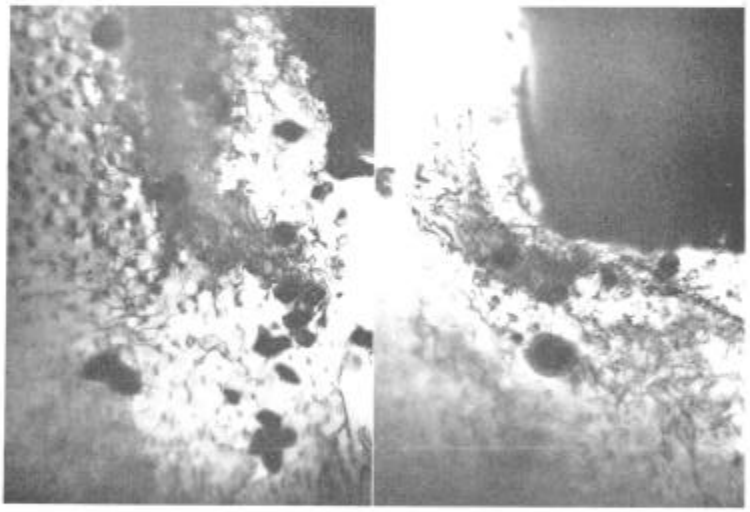

Fig.24. Nimonic 90, constrained specimen thermally cycled for 100 cycles at a maximum cycle temperature of 900°C. Fracture was first observed after 50 cycles. Note that small particles of $M_{23}C_6$ have nucleated in the vicinity of the massive particle of TiC, and there are sub-boundary networks in the γ'-free region adjacent to these particles. X25,000

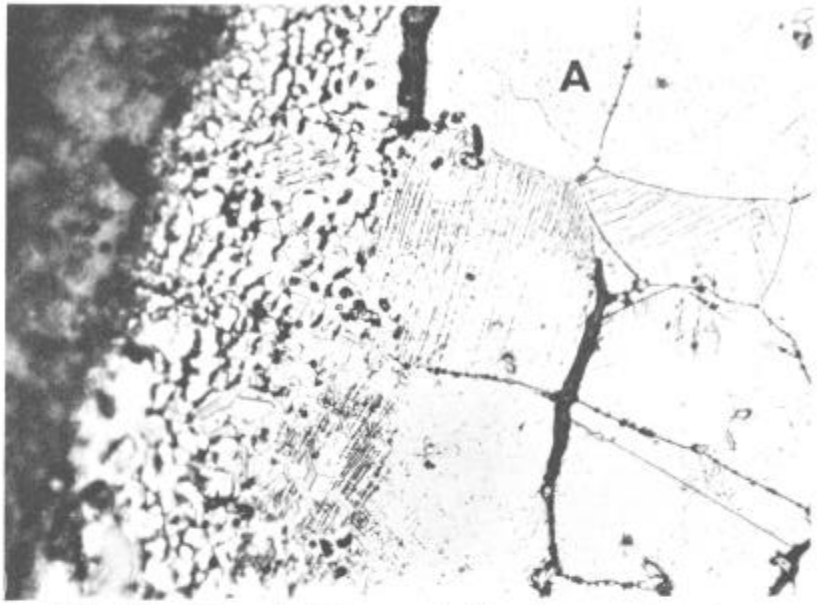

Fig.25. Nimonic 90, optical micrograph of fractured area of constrained specimen thermally fatigued at a maximum cycle temperature of 900°C. X550

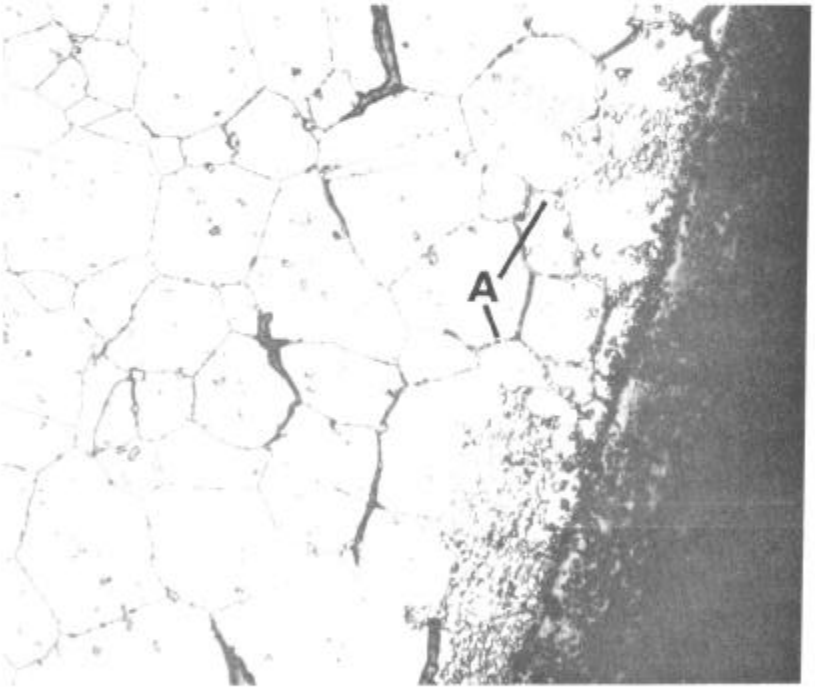

Fig.26. Nimonic 90, optical micrograph of fractured area of constrained specimen thermally fatigued at a maximum cycle temperature of 900°C. X250